
Article:
Zhan, M., Guo, J., Fu, M.W. et al. (4 more authors) (2018) Formation mechanism and control of flaring in forward tube spinning. International Journal of Advanced Manufacturing Technology, 94 (1-4). pp. 59-72. ISSN 0268-3768

https://doi.org/10.1007/s00170-017-0690-6

International Journal of Advanced Manufacturing Technology, 2017
DOI 10.1007/s00170-017-0690-6

Formation mechanism and control of flaring in forward tube spinning

M. Zhan[1*], J. Guo[1], M.W. Fu[2], R. Li[1], P.F. Gao[1], H. Long[3], F. Ma[4]

*Mei Zhan zhanmei@nwpu.edu.cn

[1]State Key Laboratory of Solidification Processing, School of Materials Science and Engineering, Northwestern Polytechnical University, Xi'an 710072, China

[2]Department of Mechanical Engineering, The Hong Kong, Polytechnic University, Hung Hom, Kowloon, Hong Kong

[3]Department of Mechanical Engineering, The University of Sheffield, Sheffield S1 3JD, UK

[4]Long March Machinery Factory, China Aerospace Science and Technology Corporation, Chengdu 610100, China

Abstract

Forward tube spinning (or flow forming) is usually employed to produce cylindrically tubular components to meet the increasing requirements for manufacturing high- performance and light-weight products at low cost and short lead-time. In forward tube spinning, flaring defect may easily occur at the opening end of tubes, which would deteriorate the quality of the spun tubular parts and reduce the material utilization. In addition, an additional operation is needed to trim away the flared end of the spun tabular parts. Efficient control of flaring formation is thus a non-trivial issue in forward tube spinning process and thus become one of the critical bottle- neck issues to be addressed in this unique forming process. In this study, the formation mechanism of flaring was systematically studied via finite element (FE) simulation and an in- depth understanding was thus established, which forms basis for control of flaring forming in forward tube spinning. Based on the simulated material flow behaviour, it is found that flaring is formed by the material in non-spun zone flowing away from the mandrel. This material flow behaviour is caused by the pile up and the decreasing stiffness of the non-spun zone. In addition, the effects of process parameters on flaring were investigated to reduce flaring. The results show that the smaller feed rate and thickness reduction per pass can reduce the maximum flaring to a certain extent, but is very limited. To increase productivity and shorten forming lead-time, an efficient method to control flaring was proposed using a pressing ring in front of the roller based on the formation mechanism of flaring. FE simulation was further used to study the feasibility and demonstrates the validity of the method in terms of reducing and even eliminating the flaring with a short production lead-time. Finally, the forward tube spinning experiments were carried out to validate the formation mechanism of flaring and the method to avoid or eliminate the flaring formation in forward tube spinning.

Keywords:

Tube spinning, Flow forming, Flaring, Forming mechanism, Flaring control and reduction

International Journal of Advanced Manufacturing Technology, 2017
DOI 10.1007/s00170-017-0690-6

1 Introduction

Tube spinning, also known as flow forming, is a forming process used to produce cylindrically tubular components [1–4]. According to the axial flow direction in tube spinning process, tube spinning is classified into two categories, namely, forward and backward spinning. In forward tube spinning process, workpiece rotates with mandrel and one or more rollers, which revolve around their own axis, move axially along the workpiece to reduce the thickness and increase the axial length of workpiece. Thus, the material flows in the same direction as that of the rollers, as shown in Fig. 1 [5]. While in backward tube spinning process, the material flows in the opposite direction to that of the rollers [6]. In most cases, forward tube spinning process is usually adopted to manufacture thin-walled tubular components with a high length- diameter ratio [7]. In this spinning process, however, flaring may occur at the opening end of workpiece (Fig. 2) [8–10]. This can easily lead to fracture at the tube end in the subsequent spinning process.

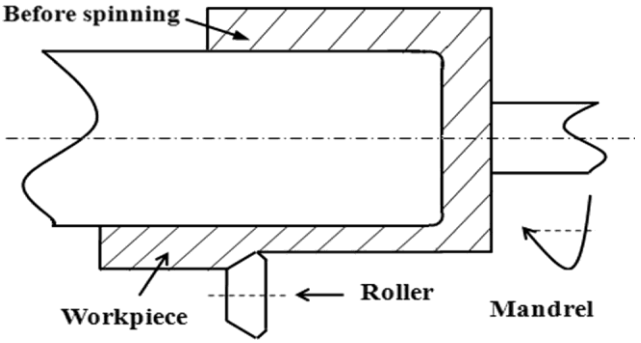

Fig. 1 Forward tube spinning

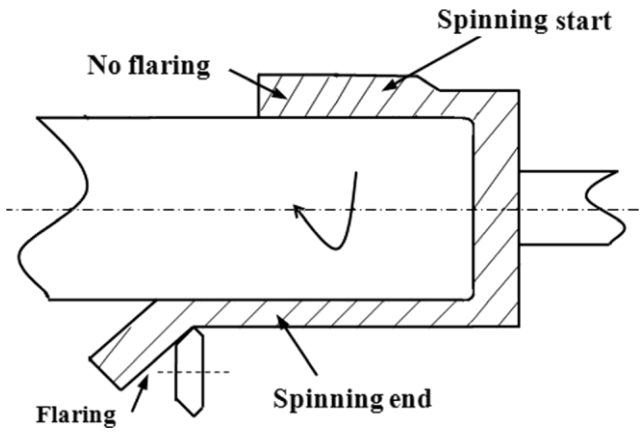

Fig. 2 Flaring formation at the end of the tube

The diameter of the flared end is much larger than that of the other parts of the tubes (Fig. 2). Flaring is thus considered to be a result of the increase in diameter (or diametrical growth) of the opening end of the tube in tube spinning process [11], and many studies have been conducted on diameter expansion than on flaring. Xu [12] noted that the diameter expansion in forward tube spinning process of steel was caused by circumferential tensile strain. Based on the elastic- plastic finite element (FE) analysis of the forward tube spinning process, Xue et al. [13] concluded that diameter expansion and flaring were both caused by the increase of circumferential strain and stress. In addition, Song et al. [14] investigated the circumferential residual stress in forward tube spinning process through FE analysis and X-ray diffraction experiments. They

found that the tensile residual stress was much larger than shear residual stress, which contributed to the diameter expansion. Furthermore, Rajan et al. [15] revealed that the diameter expansion is a function of the ratio of the circumferential contact length to the axial contact length according to the experiments by high strength SAE 4130 steel tubes and the smaller the ratio or the larger the thickness reduction, the greater the diameter expansion. Through flow forming experiments using the annealed AA6061 tubes, Davidson et al. [16] found that a roller feed rate in the range of 50–100 mm/min and a minimal gap between mandrel and workpiece are beneficial for avoiding diameter expansion. Fazeli et al. [17] figured out that the lower thickness reduction with the thinner preform thickness, the higher feed rate of rollers, the slower mandrel rotational speed, and further the lower solution treatment time facilitate obtaining the smaller internal diameter growth and wall thickness change in spinning of 2024 aluminium alloy tube. Moreover, Molladavoudi et al. [7] concluded that the diameter growth increases with the increment of thick- ness reduction in tube spinning process.

These prior arts were mainly focused on diameter expansion occurring in the deforming zone in tube spinning process, which experiences strong constraints from rollers and the spun and non-spun zones. While flaring occurs at the opening end of the tubes in the final spinning stage, it may experience the constraints different from those in diameter expansion [18]. This difference means that the forming mechanism and deformation behaviours influencing flaring occurrence might not be the same as those in diameter expansion and thus need to be systematically studied and investigated. On the other hand, how to control flaring and further to avoid it in forward tube spinning process is a critical and non-trivial issue, due to the lack of in-depth understanding of the formation mechanism of flaring and there are no effective methods to control and avoid it. The present solution is to cut off the flared end of tubes, which would reduce material utilization and increase production lead-time and cost.

In this research, the flaring formation mechanism and its evolution in tube spinning process were systematically studied by physical experiments and finite element (FE) simulation. The effects of various process parameters on flaring formation were thoroughly explored and investigated. Based on the systematic and epistemological understanding established via these explorations, an efficient method to control flaring formation was proposed. The efficiency of developed method was validated by experiment and it provides a solution for addressing this issue in industries.

2 Simulation preparation and physical experiment

To reveal the instantaneous flaring formation mechanism and the material flow which lead to the formation of flaring, FE simulation was employed as it can reveal the instantaneous deformation and flow of material, which is generally impossible for physical experiment. In addition, FE simulation has been proven to be an efficient tool for addressing metal forming design in terms of metal formed part design, process determination, tooling design and product quality control and assurance [19–21]. In tandem with this, the extensive FE simulations were conducted, together with physical experiments to study the flaring systematically in forward tube spinning process.

International Journal of Advanced Manufacturing Technology, 2017
DOI 10.1007/s00170-017-0690-6

2.1 Material

The tube material used in this study was an Al-Mn1-Cu aluminium alloy and its composition was listed in Table 1. The mechanical properties were determined by tension test and the true stress-strain curve was shown in Fig. 3.

By using the true stress-strain curve, the material constitutive model was represented by Eq. (1),

$$\sigma = \sigma_S + B\varepsilon^n \qquad Eq.(1)$$

where σ and ε are the stress and strain, respectively. σs is the initial yield stress and B and n are material constants. The material constants used in this study were shown in Table 2.

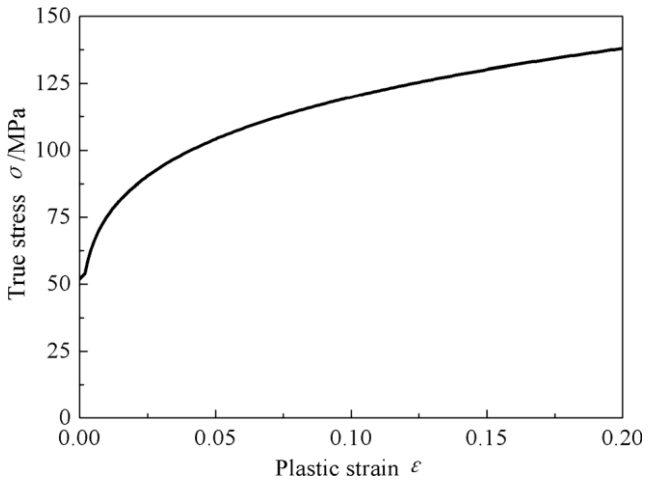

Fig. 3 True stress- strain curve of Al-Mn1-Cu aluminium alloy

Table 1 Chemical composition of Al-Mn1-Cu aluminium alloy

Element	Al	Mn	Cu	Si	Fe	Zn
Content (wt%)	Matrix	1.2	0.2	0.6	0.7	0.1

Table 2 Property parameters of Al-Mn1- Cu aluminium alloy

Parameters	Values
Elastic modulus E (GPa)	69.08
Poisson ratio v	0.33
Initial yield stress σS (MPa)	52
Material constant B (MPa)	153
Material constant n	0.21

2.2 Simulation of forward tube spinning process

In forward tube spinning, there exists a large plastic deformation with the nonlinearities of material, geometry and boundary. Abaqus/Explicit code was used and the three-dimensional (3D) elastic-plastic FE model was shown in Fig. 4. In the model, the tube was set as a deformable body and was meshed by an 8-node reduced integration brick element. Four layer elements were adopted along the thickness direction of the tube blank, which are sufficient to model the deformation in thickness direction in spinning process

International Journal of Advanced Manufacturing Technology, 2017
DOI 10.1007/s00170-017-0690-6

[22–24]. In addition, adaptive mesh control was applied to remesh the tube work- piece during the process. The roller and the mandrel were set as rigid body. A coupling constraint was applied to the fixed end of the tube to synchronize the tube and mandrel rotations. A velocity boundary was applied to control the rotation of mandrel and the axial feed motion of the roller. In addition, the Coulomb's friction model was used to represent the sliding effect between tube blank, rollers and mandrel. The friction coefficients between blank, mandrel, and roller were all set as 0.1 [25]. The forming parameters are listed in Table 3.

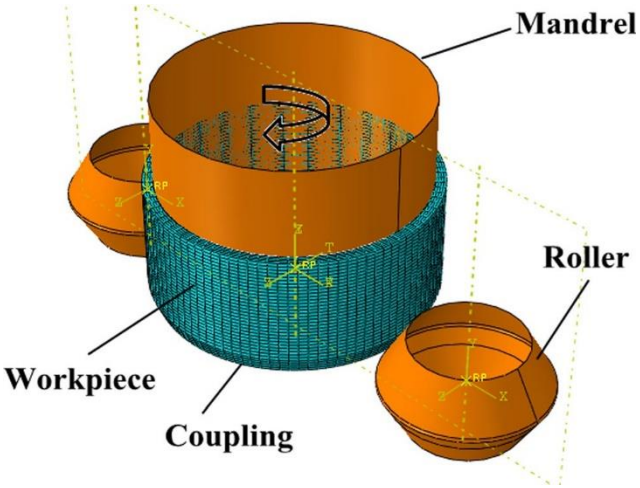

Fig. 4 3D elastic-plastic FE model for forward tube spinning

Table 3 Forming parameters in FE simulation

Parameters	Values	Parameters	Values
Tube blank length (mm)	120	Roller feed rate f (mm/r)	1.5
Inner diameter of blank	320	Spinning pass n_S	1
Blank thickness (mm)	12	Total thickness reduction ψ	40
Roller diameter (mm)	200	Rotation speed (r/min)	100
Roller attack angle (°)	30	Friction coefficient μ	0.1
Roller fillet radii (mm)	5	Roller feed stroke (mm)	140

Theoretically, more accurate simulation results are expected by using the finer mesh, but at the cost of computation time and cost. To reasonably determine the mesh size of tube blank, the calculation accuracy and the time and cost of three FE models with mesh sizes of 4, 3 and 2 mm in the axial-hoop plane were compared. Table 4 shows that the maximum Mises stress, the maximum equivalent strain and computation time are all increased with the decrease of mesh size. Furthermore, the values of the maximum Mises stress were not found to change significantly under various mesh sizes. On the other hand, the difference of the maximum equivalent strain for the mesh size of 4 and 3 mm is 12.3%, while that for the mesh size of 3 and 2 mm is only 4.5%. These differences indicate that a mesh size less than 3 mm is good enough to simulate the tube spinning process. Considering the computational time with the mesh size of 3 mm is 39.2% less than that with the mesh size of 2 mm, the mesh size of 3 mm was thus adopted in stimulation.

In addition to the mesh size, the mass scaling factor also significantly affects the simulation results. To choose a reason- able mass scaling factor in simulation, the calculation accuracy, stability and efficiency of the model, and the internal energy, kinetic energy and computation time with four mass scaling factors were investigated, as shown in Fig. 5. In the figure, the internal energy is found to be increased with spinning time. With the decrease of mass scaling factor, the difference of the internal energy with various mass scaling factors is increased with time and the maximum relative difference of the internal energy in different scenarios is approximately 8.1% in the final spinning stage. Figure 5b shows that the kinetic energies under various scaling factors are all increased significantly in the initial spinning stage and then tend to be almost stable in the subsequent spinning stage. In addition, Fig. 5b also shows the increasing fluctuation of the kinetic energy in the stable stage with the increase of the mass scaling factor, which illustrates that the dynamic effect becomes increasingly significant with the increasing mass scaling. These variations of the internal and kinetic energies lead to the decrease of the ratio of kinetic energy to internal energy with spinning time, and its increase with the mass scaling factor, as shown in Fig. 5c. Furthermore, Fig. 5c also shows that the initial stage in which the ratio is decreased sharply to 5% become shorter with the decrease of mass scaling factor. The curves with the mass scaling factor of 3500 and 6400 show a longer stage, in which the ratio of 5% is larger than those with the mass scaling factor of 900 and 400. This indicates that a smaller mass scaling factor facilitates a more rapid transition to the stable spinning process. Figure 5d shows that with the increase of mass scaling factor, computation time decreases remarkably. For a reliable FE simulation of the spinning process, the maximum ratio of kinetic energy to internal energy must be less than 10%, and the kinetic energy curve must be free of any sudden fluctuation [26–30]. Based on this discussion, it can be concluded that the energy variation under the mass scaling factor of 900 and 400 are within the limit for a reliable FE simulation of the spinning process. This indicates that dynamic effect in the spinning process is not significant and can be negligible in these two mass scaling factors. Furthermore, considering that the computation time with the mass scaling factor of 400 is approximately 1.5 times longer than that with the mass scaling factor of 900, the rational mass scaling factor for simulation was confirmed as 900.

Table 4 Simulation results under different mesh sizes

Mesh size	4 mm	3 mm	2 mm
Maximum Mises stress (MPa)	238.1	240.7	241.3
Maximum equivalent strain	4.569	5.210	5.453
CPU time (h)	99	248	408

2.3 Forward tube spinning experiment

The forward tube spinning experiments were conducted on a CZ900/2CNC spinning machine, as shown in Fig. 6. The blanks used in the experiments were cut from tubes. To make the tube blank rotate synchronously with the mandrel, a fixed end was manufactured at the bottom end of the blank and a designed fixed die was inserted into the fixed end, as shown in Fig. 7. The fixed die is connected to the blank by inserting the fixed die into two through holes manufactured in the fixed end of the blank. During the experiment, the tailstock was forced to press the fixed die to make the tube blank rotate synchronously with the mandrel. The forming parameters were the same as those in Table 3. The blank surface was coated with MoS_2 as lubricant. Furthermore, a coolant was also used through the experiment process to avoid rapid temperature rise of spun tube.

International Journal of Advanced Manufacturing Technology, 2017
DOI 10.1007/s00170-017-0690-6

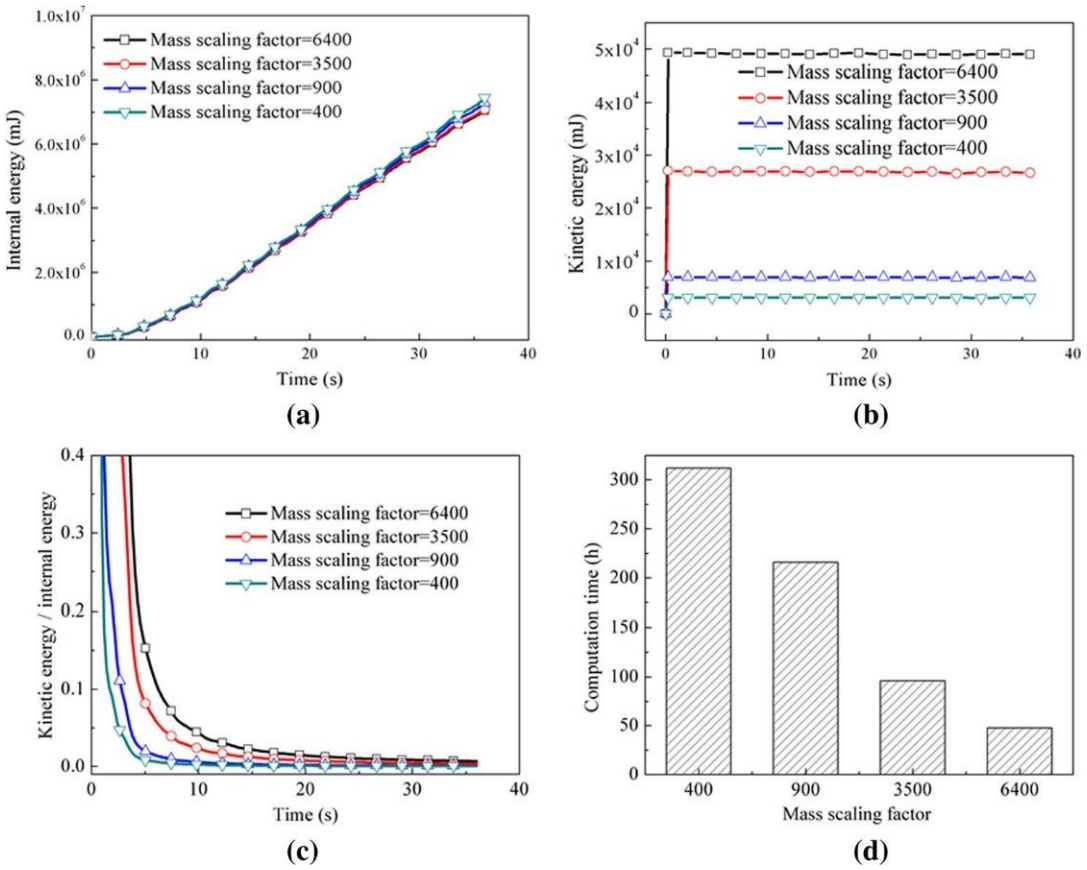

Fig. 5 Variations of (a) internal energy, (b) kinetic energy, (c) ratio of kinetic energy to internal energy, and (d) computation times under different mass scaling factors

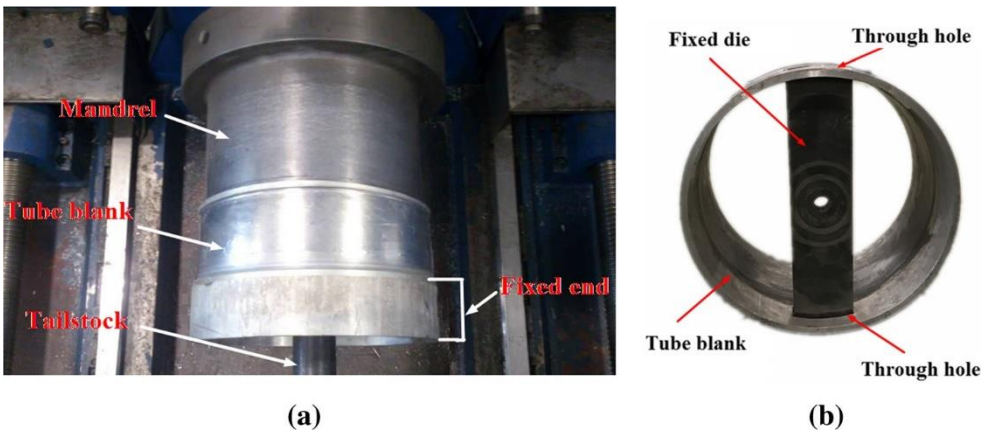

Fig. 6 Tube spinning experiments. (a) Tube blank on the mandrel. (b) The assembly of the fixed die and blank

International Journal of Advanced Manufacturing Technology, 2017
DOI 10.1007/s00170-017-0690-6

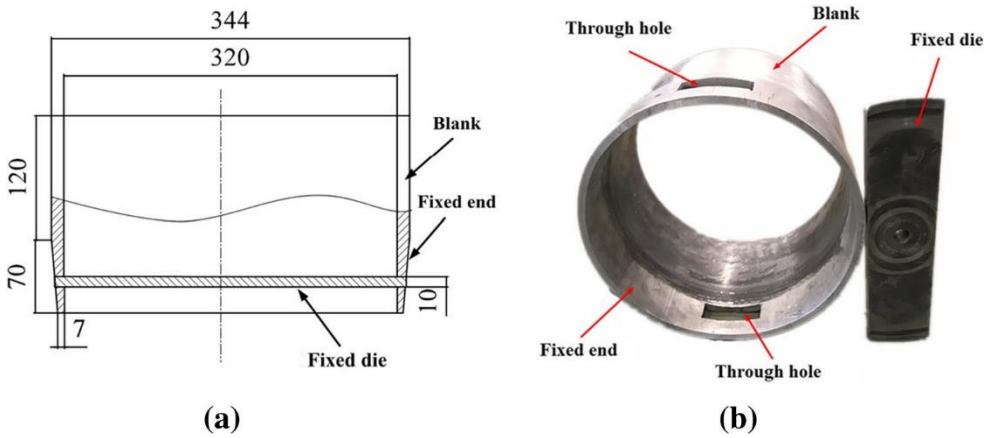

Fig. 7 Fixed end and tube blank. (a) Sketch. (b) Experimental scenario

3 Flaring formation and influencing parameters

The formation of flaring in forward tube spinning process and the effects of process parameters on flaring are the focus and they were systematically studied and presented in the following.

3.1 Formation mechanism

Based on the FE simulation of forward tube spinning process, the formation of flaring can be divided into two main stages, as shown in Fig. 8. Firstly, when the roller moves forward, the material in front of the roller accumulates and pile up is formed. Due to the formation of pile up, the material in front of the roller further flows upwards and backwards and moves away from the mandrel. Bulge up is then formed between the flowing material and mandrel. At the same time, the material in the non-spun zone still flows forwards and shows no tendency to move away from the mandrel. Then, the roller keeps moving forwards, the material in the non-spun zone moves away from the mandrel and a gap is formed between the material and mandrel and stage 2 begins. In stage 2, due to the formation of pile up, the material still flows upwards and the material in front of the roller keeps moving away from the mandrel. Meanwhile, due to the formation of bulge up and the decreasing length of the non-spun zone, the stiffness of the non-spun zone significantly decreases. When the stiffness of the non-spun zone decreases to a certain value, the material in the non-spun zone is affected by the pile up. It flows up- wards and forwards and moves away from the mandrel. This flow pattern finally develops a flaring and the maximum flaring would appear when pile up disappears, as shown in Fig. 8.

3.2 Flaring influencing parameters

Based on the revealed flaring formation mechanism, it is firstly suggested in this research to introduce the optimized parameters to make the material just flow forwards along the mandrel for the purpose to avoid the formation of flaring. Therefore, based on the FE model established in Section 2.2, a group of simulations was designed using the single factor analysis method, as shown in Table 5, to study the effects of process parameters (roller feed rate, roller fillet radii, roller attack angle, thickness reduction and thickness distribution in multiple passes) on the evolution and formation of flaring and also to control flaring in the process. The flaring was evaluated by the flaring angle and the axial length of flaring. The larger flaring angle and axial length indicate that the flaring is more severe.

International Journal of Advanced Manufacturing Technology, 2017
DOI 10.1007/s00170-017-0690-6

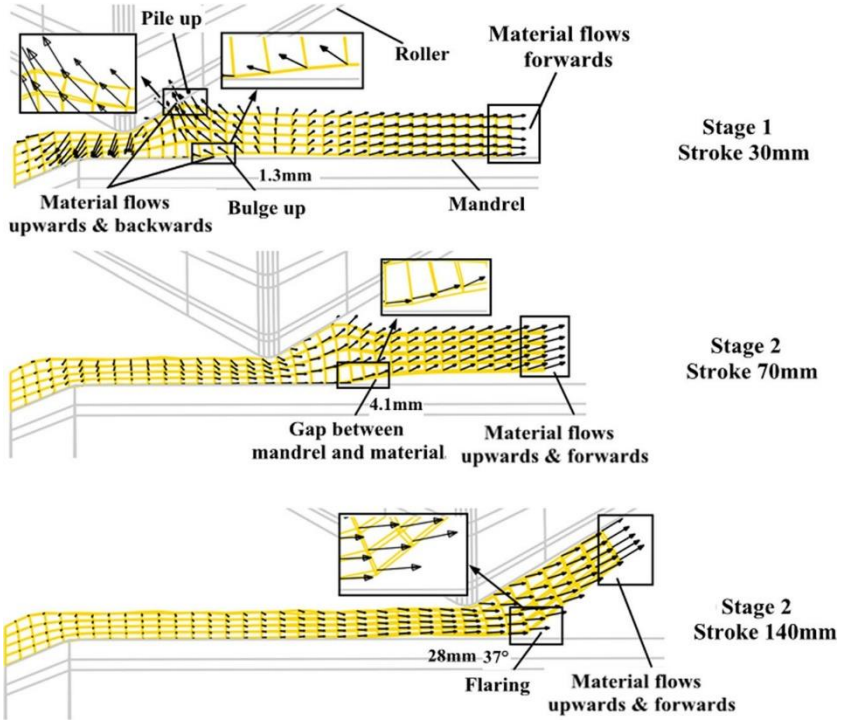

Fig. 8 Formation mechanism of flaring in forward tube spinning process

Table 5 Research plan for single factor analysis

No. Parameters	Roller feed rate f (mm/r)	Roller attack angle α (°)	Roller fillet radii Rr (mm)	Spinning pass ns	Reduction per pass ψi (%)	Total reduction ψ (%)
1	0.5	30	5	1	40	40
2	1	30	5	1	40	40
3	1.5	20	5	1	40	40
4	1.5	25	5	1	40	40
5	1.5	30	1.5	1	40	40
6	1.5	30	3	1	40	40
7	1.5	30	5	1	20	20
8	1.5	30	5	1	60	60
9	1.5	30	5	3	20	60

3.2.1 Effect of roller feed rate

Figure 9 shows the simulation results of the material flow behaviour with different feed rates. When the feed rate is 0.5 mm/r, the material under the roller does not have the tendency to move away from the mandrel before the feed stroke of 70 mm, though pile up is already formed. Thus, no bulge up and gap is formed. But the flaring is formed directly when the non-spun zone decreases to a certain length, in which the stiffness of non-spun zone is reduced and the non-spun zone is being affected by the pile up and the material flows up- wards. As the non-spun zone has a better stiffness without bulge up and gap. The flaring is formed with a shorter non- spun length compared with those under the larger feed rate. The flaring angle at the feed stroke of 140 mm is much smaller than that under the feed rate of 1 and 1.5 mm/r. When the feed rate is 1 mm/r, the bulge up, gap and flaring are formed, which are smaller than those under the feed rate of 1.5 mm/r (Fig. 8). This is due to that under a smaller feed rate, the material smoothly

flows along the axial direction, resulting in the smaller pile up. With the smaller pile up, the trend of material flowing upwards also decreases. Furthermore, it needs to be noted that the flaring would keep growing when the feed stroke exceeds 140 mm under the smaller feed rate of 0.5 and 1 mm/r, as shown in Fig. 9. The maximum flaring is found to appear with the larger feed stroke under smaller feed rate. The maximum flaring angle and axial length are all found to decrease with the decrease of feed rate, which indicates that smaller feed rate is helpful to control flaring formation.

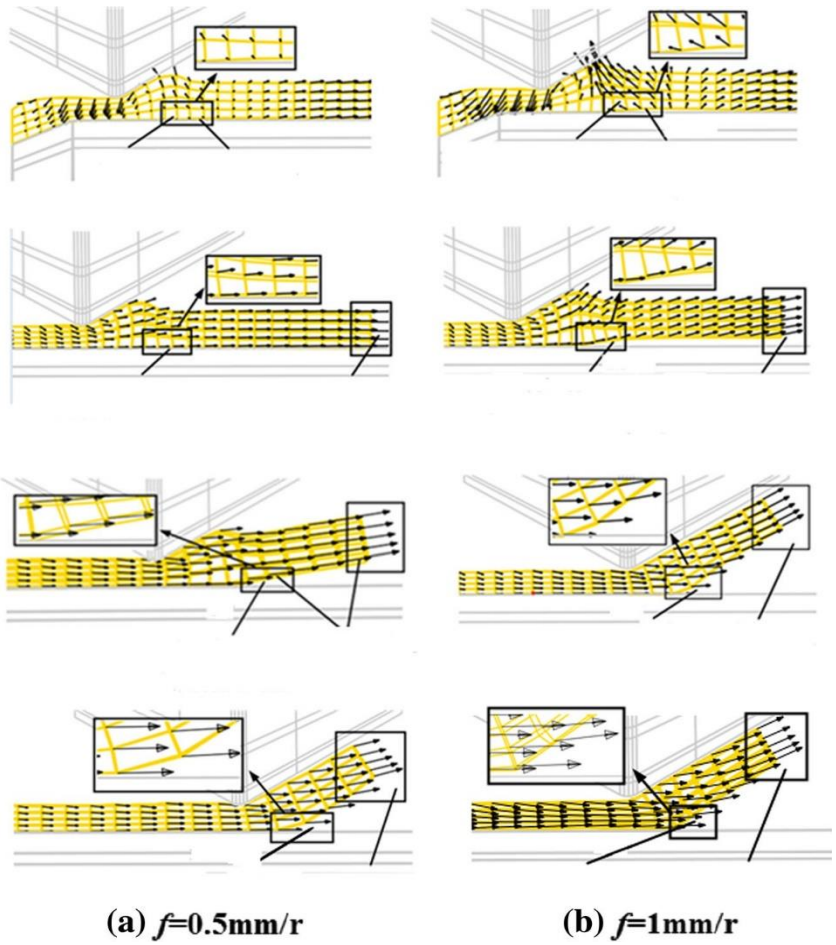

Fig. 9 Material flows in different feed rates. (a) f = 0.5 mm/r. (b) f = 1 mm/r

3.2.2 Effect of roller attack angle

Figure 10 shows the simulation results of the material flow with different attack angles. It is found that the bulge up, gap and flaring are formed under different attack angles. The bulge up and pile up decrease with the increase of attack angle. This is caused by the fact that with the smaller attack angle, the contact length between the roller and blank increases, leading to the decrease of the axial material flow and the increase of circumferential material flow, which in turn causes a larger bulge up and gap. However, under a smaller attack angle, the larger bulge up and gap would not lead to a larger flaring angle. As the flaring development is constrained by rollers and when the flaring grows to the roller attack angle, it will stop increasing. Thus, the maximum flaring angle under larger attack angle is larger than those under the smaller attack angles. However, the maximum flaring axial length under the larger attack angle is found to be smaller than those under the smaller attack angles. Those results indicate that the smaller or larger attack angle would lead to a more severe flaring.

International Journal of Advanced Manufacturing Technology, 2017
DOI 10.1007/s00170-017-0690-6

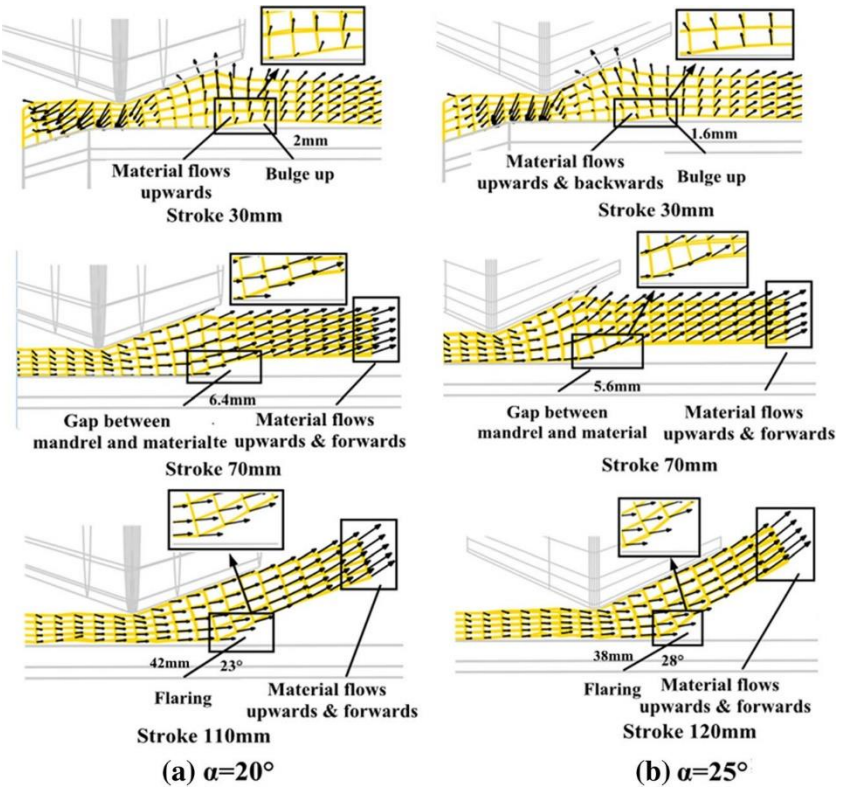

Fig. 10 Material flows in different attack angles. (a) α = 20°. (b) α = 25°

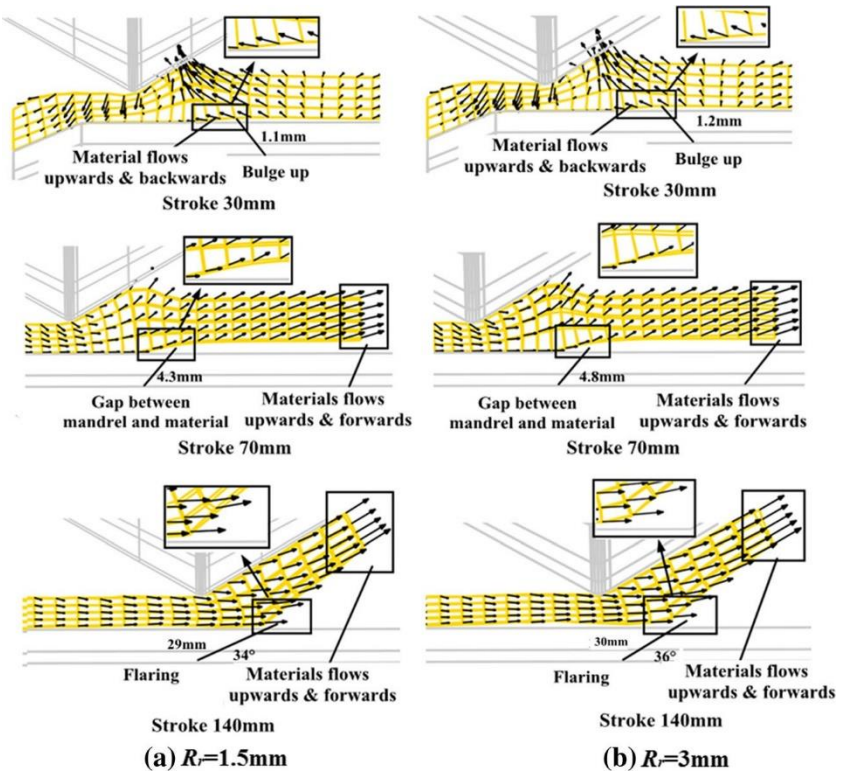

Fig. 11 Material flow in different roller fillet radii. (a) Rr = 1.5mm. (b) Rr = 3mm

International Journal of Advanced Manufacturing Technology, 2017
DOI 10.1007/s00170-017-0690-6

3.2.3 Effect of roller fillet radii

Figure 11 shows the simulation results of the material flow behaviour with different roller fillet radii. The maximum flaring all appears at the feed stroke of 140 mm. It is found that the maximum flaring angle and axial length all increase slightly with the increase of roller fillet radii. This is because the con- tact area between the roller and the workpiece increase with the increase of roller fillet radii. An increased amount of material under the contact area implies that more materials must flow in the axial direction, resulting in a greater material accumulation in front of the roller, which leads to a slight increase in the pile up in front of the roller and thus an in- creased bulge up, gap and flaring angle.

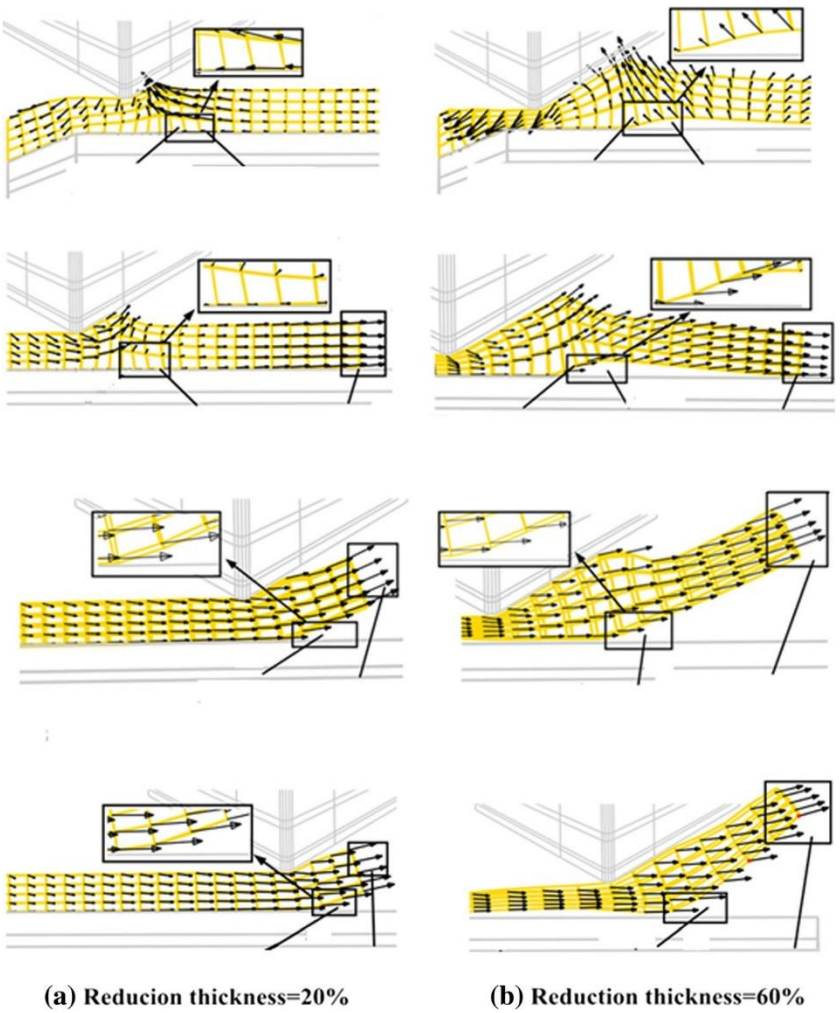

Fig. 12 Material flows in different thickness reductions. (a) 20%. (b) 60%

3.2.4 Effect of thickness reduction

The thickness reduction in a single pass on flaring and the total thickness reduction and its allocation in multiple passes have an effect on flaring formation and thus need to be studied.

Effect of thickness reduction in single pass Figure 12 shows the simulation results of the material flows with different thickness reductions. When the thickness reduction is 20%, the bulge up and gap is not formed before the feed stroke of 70 mm, which is caused by the fact that a small thickness reduction results in a small pile up. The small pile up would not make the material near the mandrel flow upwards. The flaring is formed in the final stage in which the stiffness of the non-spun zone decreases to a certain value,

being affected by the pile up. At the feed stroke of 140 mm, the flaring is found to be smaller than those under the thickness reductions of 40 and 60%. Furthermore, the maximum flaring and axial length are also found to be smaller than those under the thick- ness reductions of 40 and 60%. When the thickness reduction is 60%, compared with the smaller thickness reduction, a larger pile up is formed under this condition and thus leads to a larger bulge and gap and finally results in a larger flaring angle and axial length. This indicates that a smaller reduction in single pass is helpful to control flaring formation.

Effect of thickness reduction in multiple pass: Figure 13 shows the simulation results of the material flows in the second and third passes under a total reduction of 60% with the same thickness reduction per pass (thickness reduction of 20%). In the second pass, it is found that a very small bulge up is formed and then gradually grows up. In the final stage of the second pass, the flaring is formed due to the decreasing length of non-spun zone. Compared with the spinning process with one single pass with the thickness reduction of 40% (Fig. 8), it can be found that the maximum flaring angle and axial length with two passes is smaller and appears with the larger feed stroke. While in the third pass, it can be clearly found that a large bulge up appears and gradually grows up, resulting in the large flaring angle and axial length. Compared with the spinning process with one single pass with the thickness reduction of 60% (Fig. 12), three passes spinning would not help decrease the flaring. For the thickness reduction of 60%, more spinning passes with a smaller thickness reduction per pass are needed for flaring control.

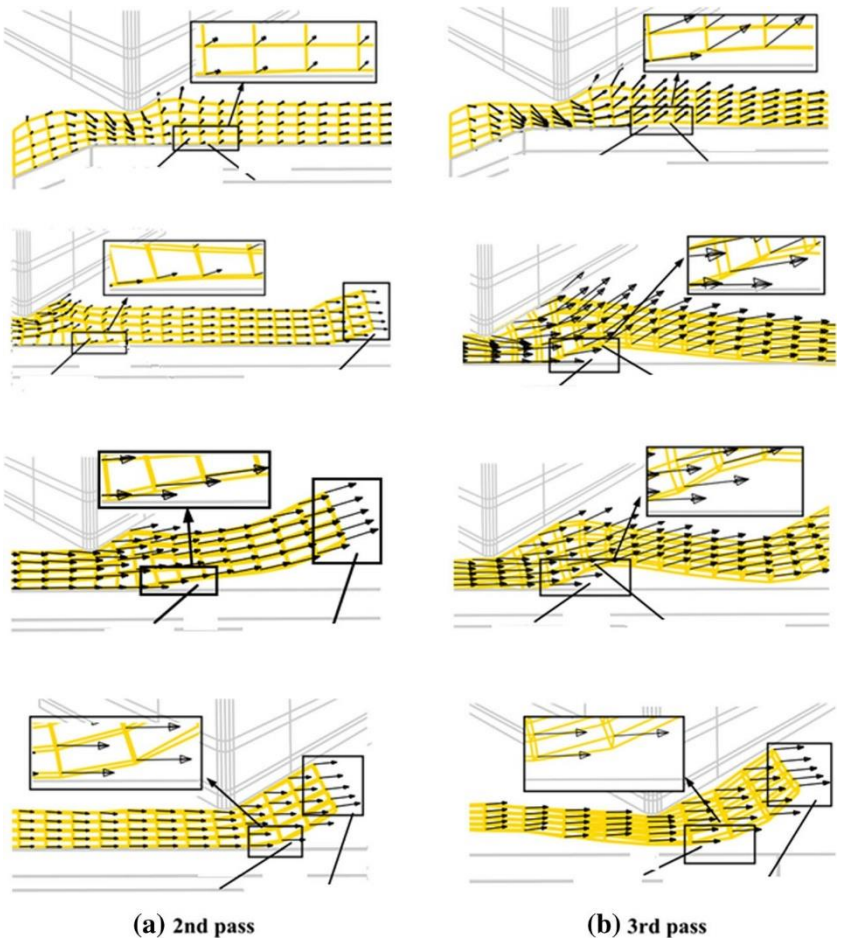

Fig. 13 Material flows in different spinning passes. (a) 2nd pass. (b) 3rd pass

International Journal of Advanced Manufacturing Technology, 2017
DOI 10.1007/s00170-017-0690-6

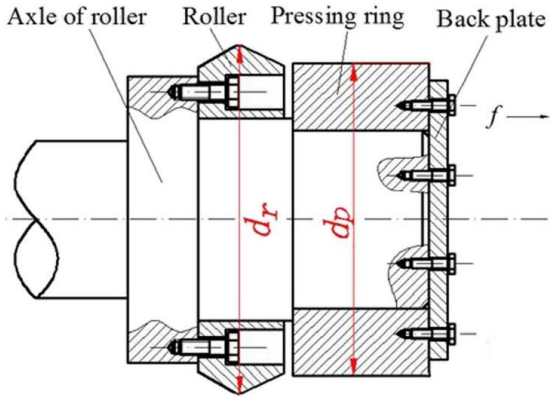

Fig. 14 Pressing ring fixed on the axle of the roller

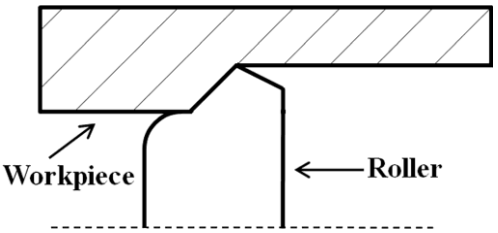

Fig. 15 Special roller suggested by Klocke and Knig [31]

4 Control and reduction of flaring

Based on the investigation of the influence of process parameters in Section 3.2, it can be concluded that the decreasing thickness reduction per pass and roller feed rate can help decrease flaring to a certain extent. However, the decrease is very limited. Furthermore, the spinning process under these parameters has a long forming lead-time. This makes it difficult to form the high-performance and light-weight tubes through spinning with a good productivity.

Therefore, a control method to efficiently reduce and even eliminate flaring in the forward tube spinning process is thus critically needed. Based on the analysis of forming mechanism in Section 3, it is known that flaring is mainly caused by pile up. Therefore, a method to control flaring formation was proposed by installing a pressing ring in front of the roller, as shown in Fig. 14. With the pressing ring is fixed in the axle of roller, it can move axially with the roller and rotate during the spinning process. Therefore, the pressing ring can suppress the material pile up in front of the roller and flow away from the mandrel.

Considering the relative positions of the pressing ring and the roller, the thickness reduction and the constraint to the pile up in front of the roller, the outside diameter of pressing ring should be slightly smaller than the difference of the diameter of roller and thickness reduction. Therefore, the outside diameter of pressing ring was determined as

$$d_p = d_r - 2\psi - mt_0 \qquad Eq.(2)$$

where d_p is the outside diameter of pressing ring, d_r stands for the roller diameter, ψ is the total thickness reduction, t_0 is the initial wall thickness of tube blank, and m is a coefficient with a range of 0.2–0.4 to define the initial gap between the press ring and the blank under different thickness reductions. The initial gap could prevent the friction caused by the unnecessary contact between the press ring and the blank in the initial stage of spinning. The length of the pressing ring can be set as approximately 3–5 times the thickness of the tube blank, since the length of the non-spun zone approximately reaches the value when flaring occurs.

In this method, the pressing ring can suppress the formation of pile up in front of the roller, finally controlling the flaring at the end of tube spinning. This method is similar to that of the special roller with a specific shape fillet, suggested by Klocke and Knig [31], as shown in Fig. 15. The separate structural design of the pressing

International Journal of Advanced Manufacturing Technology, 2017
DOI 10.1007/s00170-017-0690-6

ring with the roller makes enables flexible matching of pressing rings to the roller with different radii. This makes the pressing ring suitable for different spinning processes with different thickness reductions, in contrast to the design of the fillet size of the special roller suggested by Klocke and Knig. The difference in the two structures indicates that the method in this study is more flexible.

To verify the feasibility of the proposed method for con- trolling flaring, a 3D FE model of forward tube spinning with a pressing ring (Fig. 16) was established, based on the 3D FE model without the pressing ring described in Section 2.2. In the model with the pressing ring, all the process parameters were the same as those in Section 2.2 and Table 3. The pressing ring was set to have a length of 45 mm and a diameter of 186.8 mm by using a coefficient m of 0.3.

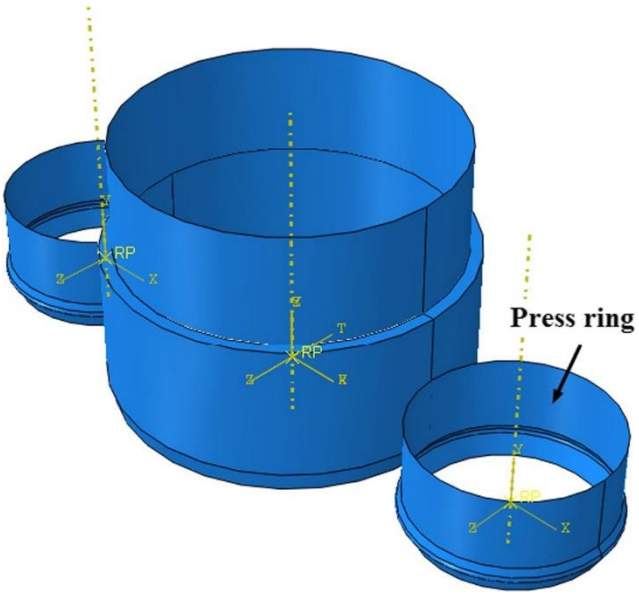

Fig. 16 3D FE model for forward tube spinning with a pressing ring

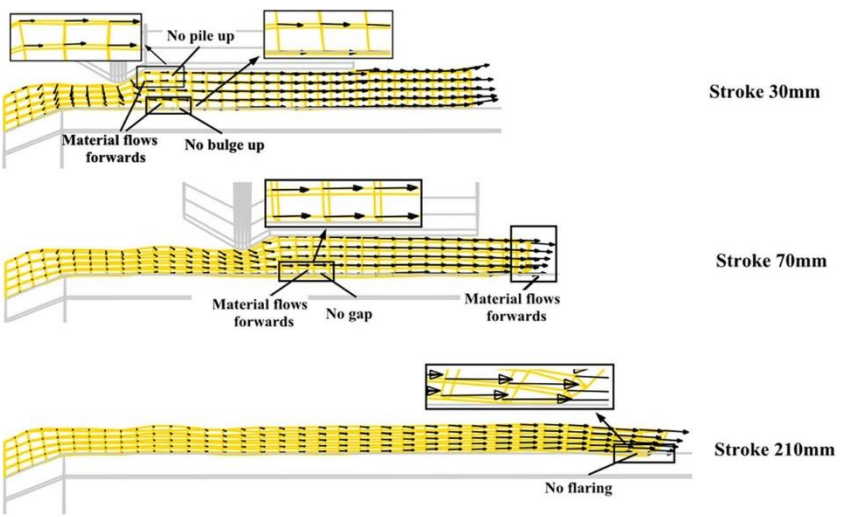

Fig. 17 Material flows with pressing ring

International Journal of Advanced Manufacturing Technology, 2017
DOI 10.1007/s00170-017-0690-6

The material flow with flaring is shown in Fig. 17. With the feed stroke of 30 mm, it is found that no pile up is formed under the action of press ring. Thus, the material under the roller flows forwards and shows no tendency of flowing up- wards, resulting in no bulge up. As roller moves forwards with the feed stroke of 70 mm, the material under the roller still moves forwards, while the material in the non-spun zone also flows forwards. Thus, no gap is formed between the material and mandrel. When the roller moves to the end of the work- piece with the feed stroke of 210 mm, it can be clearly found that no flaring is formed, indicating that the pressing ring can prevent the formation of flaring efficiently.

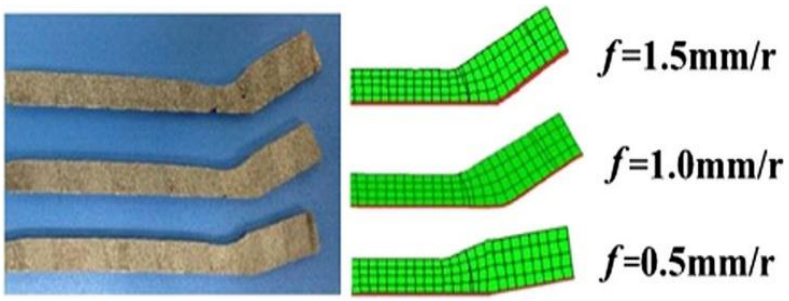

Fig. 18 Flaring got in experiments and simulations at the same feed stroke

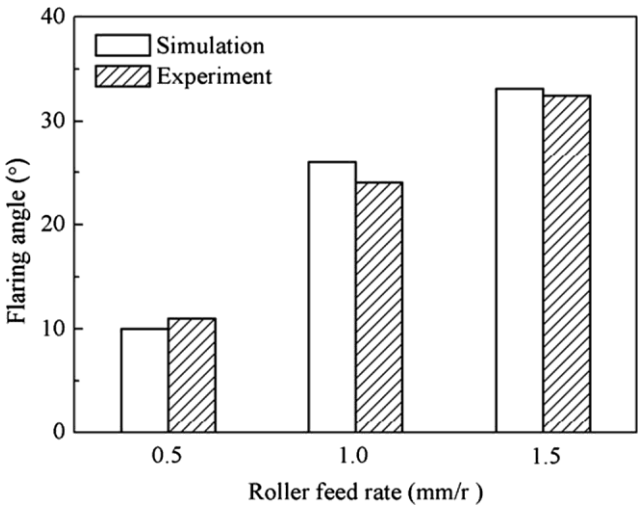

Fig. 19 Comparisons of flaring between experiments and simulations

(a) (b)

Fig. 20 The pressing ring used and the spun tubes with pressing ring. (a) Pressing ring. (b) Spun tubes with pressing ring

International Journal of Advanced Manufacturing Technology, 2017
DOI 10.1007/s00170-017-0690-6

5 Experiment study

The forward tube spinning experiments with the roller feed rate of 0.5, 1.0 and 1.5 mm/r were conducted as case studies in this research. The longitude section of the spun tube with the feed stroke of 140 mm were shown in Fig. 18. It can be found that flaring also occurs in the experiments, and flaring in- creases with feed rate. The flaring angles identified in experiments are found to show no large difference with those got in simulations, as shown in Fig. 19.

To avoid flaring, a pressing ring was designed based on the simulation in Section 4, as shown in Fig. 20a. Figure 20b shows the spun tube with pressing ring. It can be found that no flaring appears in the spun tube, which indicates that the introduction of pressing ring into the spinning system is an effective method to reduce and even eliminate flaring. It is worth noting that the spinning experiment was accomplished under a large roller feed rate of 1.5 mm/r, and a large thickness reduction in a single pass of 60%. This further indicates that it is an efficient method to reduce and even eliminate flaring under a large roller feed rate and thickness reduction per pass with high productivity.

6 Conclusions

The formation mechanism, influencing parameters and control method of flaring were investigated through FE simulation on the forward tube spinning of Al-Mn1-Cu aluminium alloy together with physical experiments. The main conclusions are drawn in the following:

1. In forward tube spinning process, the formation of flaring is formed as the material in the non-spun zone flows away from the mandrel. This material flow is caused by the pile up and the decreasing non-spun zone stiffness.

2. The roller feed rate and thickness reduction per pass are the key factors influencing flaring formation. For the spinning process with a large total thickness reduction, it is useful to use multiple passes and the small thickness reduction per pass and roller feed rate can decrease flaring to a certain extent. However, the flaring decrease is very limited and such a spinning process has a long forming lead-time.

3. A method to reduce flaring by introducing a pressing ring in front of the roller in spinning system was proposed to control flaring via suppressing the pile up of material in spinning process. The FE simulations and experiments show that it is an efficient method for reducing and eliminating flaring with short forming time and thus provides a promising method for industries to address this issue.

4. The formation mechanism of flaring and the deformation behaviours affected by various process parameters were revealed by FE simulation and physical experiments, which provide an in-depth understanding of spinning and help process determination and tooling design in fabrication of spinning parts.

International Journal of Advanced Manufacturing Technology, 2017
DOI 10.1007/s00170-017-0690-6

Acknowledgements

The authors acknowledge the funding support from the National Science Fund for Distinguished Young Scholars of China (Project 51625505), National Science Fund for Excellent Young Scholars of China (Project 51222509), Key Program Project of the Joint Fund of Astronomy and National Natural Science Foundation of China (Project U1537203) and Research Fund of the State Key Laboratory of Solidification Processing (Projects 97-QZ-2014 and 90-QP-2013). The authors also acknowledge the partial support of the EU FP7 Marie Curie International Research Staff Exchange Scheme (IRSES, MatProFuture, Project 318968).

References

1. Wong CC, Dean TA, Lin JG (2003) A review of spinning, shear forming and flow forming processes. Int J Mach Tools Manuf 43(14):1419–1435
2. Music O, Allwood JM, Kawai K (2010) A review of the mechanics of metal spinning. J Mater Process Technol 210(1):3–23
3. Parsa MH, Pazooki AMA, Ahmadabadi MN (2009) Flow-forming and flow formability simulation. Inter J Adv Manuf Tech 42(5–6): 463–473
4. Xia QX, Cheng XQ, Long H, Ruan F (2012) Finite element anal- ysis and experimental investigation on deformation mechanism of non-axisymmetric tube spinning. Int J Adv Manuf Technol 59:263–272
5. Xu WC, Zhao XK, Ma H, Shan DB, Lin H (2016) Influence of roller distribution modes on spinning force during tube spinning. Inter J of Mech Sci 113:10–25
6. Zhao GY, Lu CJ, Zhang RY, Guo ZH, Zhang MY (2017) Uneven plastic deformation behavior of high-strength cast aluminum alloy tube in multi-pass hot power backward spinning. Inter J Adv Manuf Tech 88(1):907–921
7. Molladavoudi HR, Djavanroodi F (2011) Experimental study of thickness reduction effects on mechanical properties and spinning accuracy of aluminum 7075-O, during flow forming. Inter J Adv Manuf Tech 52(9):949–957
8. Luo B, Li X, Zhang X, Luo Y (2015) Drum instability of thinning spinning ultra thin-walled tubes with large diameter-to-thickness ratio. J Cent South Univ 22(7):2456–2462
9. Zhao XK, Xu WC, Chen Y, Ma H, Shan DB, Lin H (2017) Fabrication of curved generatrix workpiece of TA15 titanium alloy by variable thickness tube spinning and flaring process. Inter J Adv Manuf Tech 88(5):1983–1992
10. Hazawi ARK, Abdel-Magied RK, Elsheikh MN (2017) An exper- imental analysis of a flaring process for tube ends using a novel spinning tool. Int J Adv Manuf Technol. doi:10.1007/s00170-017-0106-7
11. Mohebbi MS, Akbarzadeh A (2010) Experimental study and FEM analysis of redundant strains in flow forming tubes. J Mater Process Technol 210(2):389–395
12. Xu D (1989) Thickness reduction spinning of the thin-walled cyl- inder with inner stiffness. In: Proceedings of the Fourth International Conference of Rotary Forming: 17-21
13. Xue KM, Wang Z, Lu Y, Li KZ (1997) Elasto-plastic FEM analysis and experimental study of diametral growth in tube spinning. J Mater Process Technol 69(1–3):172–175

14. Song X, Fong KS, Oon SR, Tiong WR, Li PF (2014) Diametrical growth in the forward flow forming process: simulation, validation, and prediction. Inter J Adv Manuf Tech 71(1- 4):207–217
15. Rajan KM, Narasimhan K (2001) An investigation of the develop- ment of defects during flow forming of high strength thin wall steel tubes. ASM J Pract Failure Anal 1(5):69–76
16. Davidson MJ, Balasubramanian K, Tagore GRN (2008) An exper- iment study on the quality of flow-formed AA6061 tubes. J Mater Process Technol 203(1):321–325
17. Fazeli AR, Ghoreishi M (2011) Statistical analysis of dimensional changes in thermomechanical tube-spinning process. Inter J Adv Manuf Tech 52(5–8):597–607
18. Rasoli MA, Abdullah A, Farzin M, Fadaei TA (2012) Influence of ultrasonic vibrations on tube spinning process. J Mater Process Technol 212(6):1443–1452
19. Fu MW (2016) Design and development of metal forming process- es and products aided by finite element simulation. Springer-Verlag London Ltd.
20. Fu MW, Yong MS, Muramatsu T (2008) Die fatigue life design and assessment via CAE simulation. Int J of Adv Manuf Technol 35: 843–851
21. Fu MW, Yong MS, Tong KK, Muramatsu T (2008) Design solution evaluation for forming product development via CAE simulation. Int J of Adv Manuf Technol 38:249–257
22. Zhang JH, Zhan M, Yang H, Jiang ZQ, Han D (2012) 3D-FE modeling for power spinning of large ellipsoidal heads with vari- able thicknesses. Comput Mater Sci 53(1):303–313
23. Zhan M, Zhang T, Yang H, Li LJ (2016) Establishment of a thermal damage model for Ti-6Al-2Zr-1Mo-1V titanium alloy and its appli- cation in the tube rolling-spinning process. Inter J Adv Manuf Technol 87(5–8):1345–1357
24. YangH, Li H, ZhanM (2010) Friction role in bending behaviors of thin-walled tube in rotary-draw-bending under small bending radii. J Mater Process Technol210(15):2273-2284
25. Ma F, Yang H, Zhan M (2010) Plastic deformation behaviors and their application in power spinning process of conical parts with transverse inner rib. J Mater Process Technol210(1):180-189
26. Abaqus Analysis User's Manual (2003) ABAQUS Inc. Version 6.4
27. Bai Q, Yang H, Zhan M (2008) Finite element modeling of power spinning of thin-walled shell with hoop inner rib. Trans Nonferrous Met Soc China 18:6-13
28. Essa K, Hartley P (2009) Numerical simulation of single and dual pass conventional spinning processes. Int J Mater Form 2:271-281
29. Huang L, Yang H, Zhan M, Hu U (2008) Numerical simulation of influence of material parameters on splitting spinning of aluminum alloy. Trans Nonferrous Met Soc China 18:674-681
30. Wang L, Long H (2011) Investigation of material deformation in multi-pass conventional metal spinning. Mater Des 32(5):2891-2899
31. Klocke F, Knig W (2006) Fertigungsverfahren Urnformen, 5th edition (German). pp 390-393